# 2.3 Å Resolution X-ray Crystal Structure of the Bisubstrate Analogue Inhibitor Salicylhydroxamic Acid Bound to Human Myeloperoxidase: A Model for a Prereaction Complex with Hydrogen Peroxide[†,‡]

Curt A. Davey and Roger E. Fenna*

*Department of Biochemistry and Molecular Biology, University of Miami Medical School, P.O. Box 016129, Miami, Florida 33101*

*Received March 8, 1996; Revised Manuscript Received June 19, 1996*[⊗]

ABSTRACT: The X-ray crystal structure of a salicylhydroxamic acid (SHA) inhibitory complex with human myeloperoxidase (MPO) has been determined at 2.3 Å resolution. The aromatic ring of the inhibitor binds to a hydrophobic region at the entrance to the distal heme pocket between heme pyrrole ring D and the side chain of Arg 239. The hydroxamic acid moiety is hydrogen bonded to both the distal histidine 95 and the adjacent glutamine 91 amide group but is not coordinated to the heme iron. SHA binding displaces three water molecules from the distal heme cavity and causes a small shift in the position of a fourth water molecule. Otherwise, there are no significant conformational differences between the active site regions of the complex and the native enzyme. The ability of the three SHA oxygen atoms to closely duplicate the hydrogen-bonding pattern of these three water molecules in the native enzyme is postulated to account for the strong binding of this inhibitor to MPO. The mode of binding of SHA to MPO provides information on the binding sites for aromatic peracid substrates that promote compound **I** formation as well as aromatic alcohols and amines that carry out single-electron reductions of compound **I**. Similarities in the hydrogen-bonding patterns of amino acid residues and water molecules in the distal heme pockets of myeloperoxidase and the nonhomologous cytochrome *c* peroxidase suggest that they may have similar mechanisms of compound **I** formation. A model is presentd for a prereaction complex of myeloperoxidase in which hydrogen peroxide is hydrogen bonded to the distal histidine, as a prerequisite for deprotonation and subsequent binding at the sixth coordination site of the heme iron.

Myeloperoxidase (MPO),[1] EC 1.11.1.7, occurring in the azurophil granules of mammalian neutrophils catalyzes the hydrogen peroxide-mediated peroxidation of chloride ion to hypochlorite (Agner, 1941; Harrison & Schultz, 1976), an effective antibacterial, antifungal, and antiviral agent (Klebanoff, 1970; Belding et al., 1970). MPO is a member of a homologous family of mammalian peroxidases that includes thyroid peroxidase, lactoperoxidase, and eosinophil peroxidase (Kimura & Ikeda-Saito, 1988; Cals et al., 1991). Myeloperoxidase is a dimer of 140 kDa, each half consisting of two polypeptides of 108 and 466 amino acids, a covalently bound heme, a bound calcium ion, and at least three sites of asparagine-linked glycosylation. A single disulfide bridge linking the two halves of the molecule at Cys 153 can be selctively cleaved to yield catalytically active hemi- MPO (Andrews & Krinsky, 1981). The X-ray crystal structure of canine MPO at 3 Å resolution (Zeng & Fenna, 1992) revealed the overall fold of the polypeptide chain and identified His 336 as the proximal ligand to the heme iron. While MPO is not homologous with the plant and fungal peroxidases, on the distal side of the heme, His 95 and Arg 239 are positioned in a manner similar to that of the catalytically active histidine and arginine residues in cytochrome *c* peroxidase (Poulos et al., 1980) and horseradish peroxidase (Welinder, 1985; Thanabal et al., 1987). A recent 2.25 Å resolution crystal structure of human MPO has shown that the heme is a derivative of protoporphyrin IX in which the methyl and vinyl groups on pyrrole ring A and the methyl group on pyrrole ring C have been modified to form covalent bonds with amino acid residues in the protein (Fenna et al., 1995). In the resting enzyme, the ferric heme has high-spin pentacoordinate spectral characteristics (Stump & Oliver, 1985) and the crystal structure confirms the absence of a sixth ligand to the heme iron. A water molecule hydrogen-bonded to the distal His 95 is positioned 3.1 Å from the iron. This distance is much greater than the 1.8−2.2 Å range seen in X-ray crystal structures of CCP with $CN^-$, $F^-$, NO, or CO ligands bound at the sixth coordination site of the heme (Edwards & Poulos, 1990).

The reaction of hydroperoxides with heme peroxidases is 5 orders of magnitude faster than with other heme proteins such as metmyoglobin (Loo & Erman, 1975; Yonetani & Schleyer, 1967). Peroxidases undergo a two-electron oxidation to form compound **I** in which a porphyrin $\pi$-cation radical contains a ferryl (+IV) iron liganded to oxygen (Dolphin et al., 1971). In the mechanism of compound **I** formation proposed for CCP, the distal histidine functions as an acid base catalyst in promoting heterolytic cleavage of peroxide, while the arginine plays a secondary role in helping to stabilize the resultant oxyferryl center of compound **I** (Poulos & Kraut, 1980a,b; Finzel et al., 1984; Miller

[†] This work was supported by a grant from the NIH (GM-49149).

[‡] Atomic coordinates for human myeloperoxidase have been deposited with The Brookhaven Protein Data Bank under access code 1MHL.

* To whom correspondence should be adressed.

[⊗] Abstract published in *Advance ACS Abstracts,* August 1, 1996.

[1] Abbreviations: MPO, myeloperoxidase; LPO, lactoperoxidase; CCP, cytochrome *c* peroxidase; HRP, horseradish peroxidase; SHA, salicylhydroxamic acid; BHA, benzylhydroxamic acid; NMR, nuclear magnetic resonance; EPR electron paramagnetic resonance; PEG, polyethylene glycol.

S0006-2960(96)00577-6 CCC: $12.00 

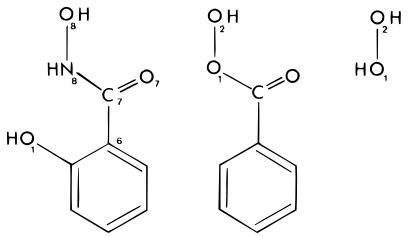

FIGURE 1: Comparison of the structures of salicylhydroxamic acid, perbenzoic acid, and hydrogen peroxide, indicating the atom nomenclature used in the text.

et al., 1994). Similar mechanisms of compound **I** formation are believed to occur in other plant and fungal heme peroxidases (Poulos et al., 1993; Kunishima et al., 1994).

Hydroxamic acids, including benzylhydroxamic acid (BHA) and SHA, are potent inhibitors of MPO (Davies & Edwards, 1989; Ikeda-Saito et al., 1991; Hori et al., 1994) as well as other mammalian (Kimura & Yamazaki, 1979; Kitagawa et al., 1983) and plant (Schonbaum, 1973; Thanabal et al., 1987) peroxidases. Schonbaum (1973) noted the similarity in structure between the hydroxamic acids and the aromatic peracids (Figure 1) that can substitute for hydrogen peroxide in promoting compound **I** formation in most heme peroxidases (Schonbaum & Lo, 1972). Additionally, both BHA and SHA, along with a wide range of aromatic alcohols and amines, act as reducing substrates for compound **I**. BHA binding to HRP has been studied extensively using $^1$H NMR (Sakurada et al., 1986; Thanabal et al., 1987; La Mar et al., 1992) and resonance Raman spectroscopy (Smulevich et al., 1991). From measurements of the proton−proton transferred nuclear Overhauser effects for the nonexchangeable ring protons of BHA bound to HRP, the binding site was located within 4 Å of the heme pyrrole ring D methyl group and 8−11 Å from the heme iron (Sakurada et al., 1986). The orientation of the aromatic ring was determined to be nearly perpendicular to the plane of the heme. La Mar et al. (1992) showed that the binding of either BHA or cyanide to HRP destabilized the binding of the other by about 3 kcal/mol. These results were interpreted in terms of competition between the hydroxyl proton of BHA and the HCN proton for hydrogen bonding to the unprotonated distal histidine.

SHA and BHA binding to MPO has been studied by both optical absorption spectroscopy (Ikeda-Saito et al., 1991) and EPR (Hori et al., 1994). The pH dependence of binding indicates the involvement of an ionizable group on the protein with a p$K_a$ of about 4. This residue is concluded to be the distal histidine, which must be in the unprotonated form for hydroxamic acid binding. Binding is accompanied by only very small changes in the optical absorption spectrum, including a shift in the Soret maximum from 429 to 431 nm. Dissociation constants of $2 \times 10^{-6}$and $5 \times 10^{-3}$ M have been determined for SHA and BHA binding to MPO, respectively (Ikeda-Saito et al., 1991). The stronger binding of SHA was suggested to indicate additional hydrogen bonding to the protein via the ring hydroxyl group of SHA. Model building based on the 3 Å structure of canine MPO revealed a hydrophobic region at the entrance to the distal cavity in which the van der Waals surface created by the heme pyrrole ring D, the $\beta$, $\gamma$, and $\delta$ carbons of Arg 239, and three nearby phenylalanines (99, 366, and 407) could readily accommodate the aromatic ring of SHA, approximately parallel with the heme and with the hydroxamic acid group positioned inside the distal cavity between the distal histidine and the heme iron. EPR studies at 77 K showed that the high-spin signal characteristic of ferric MPO is replaced by both high-spin and low-spin components upon SHA binding (Hori et al., 1994). These observations led to the suggestion that the hydroxamic acid group provided a sixth ligand to the iron, although the room-temperature optical spectra of the complex retained characteristics of a pentacoordinate high-spin heme (Ikeda-Saito et al., 1991). In this paper, we describe the first X-ray crystallographic structure of a peroxidase−hydroxamic acid complex and discuss the implications for characterizing the binding of both aromatic peracid substrates that promote compound **I** formation and aromatic alcohols and amines that can subsequently reduce compound **I** to the resting ferric heme enzyme.

## EXPERIMENTAL METHODS

*Crystallization*. Human myeloperoxidase isoform *c* was a generous gift from Dr. Nils Peder Willassen, Department of Biochemistry, University of Tromso, Norway. Since crystals of human MPO cracked when exposed to micromolar concentrations of SHA, cocrystallization was performed. Crystals were grown by a method similar to that first described by Sutton et al. (1988). Typically, 8 $\mu$L hanging droplets containing 20 mg/mL MPO, 50 mM sodium acetate (pH 5.0), 50 mM ammonium sulfate, 10 mM calcium chloride, 8% PEG 8K, and 2 mM SHA were equilibrated with 1 mL reservoirs containing 0.2 M sodium chloride. Since de novo nucleation of this crystal form rarely takes place, seeding was routinely used for all crystallizations. Crystal growth was promoted by periodically raising the reservoir salt concentration to a final level of about 0.4 M. Crystallization was carried out in a temperature-controlled room at 65 °F. Crystals grew as very thin plates which rarely reached thicknesses of greater than 0.05 mm. For this reason, it was found necessary to mount the crystals in glass capillaries in which a flat platform had been created through the application of a red hot metal spatula.

*X-ray Data Collection*. X-ray diffraction data to 2.3 Å resolution were recorded using a Molecular Structure Corp. R-axis II image plate detector mounted on a Rigaku rotating anode X-ray generator fitted with a graphite monochromator and operated at 60 kV and 100 mA in The Department of Biochemistry and Biophysics at Florida State University in Tallahassee. Three crystals were used to record 213 661 intensities which were scaled and merged using the PROCESS software package (Molecular Structure Corp.) to give a unique set of 54 275 amplitudes comprising 90% of the theoretical total to 2.3 Å. The merging *R*-factor was 5.7%. All of the data were measured at room temperature with a crystal to detector distance of 104 mm for the first crystal and 89 mm for the second and third crystals.

*Structure Determination and Refinement*. The human MPO starting model consisted of 9424 non-hydrogen atoms and 423 water molecules. This model had been refined to a crystallographic *R*-factor of 16% with rms deviations from ideality for bond lengths and angles of 0.013 Å and 3.0° using X-ray diffraction data to 2.25 Å resolution (Fenna et al., 1995). Initially, a difference map was calculated using $F_{o(MPO-SHA)} - F_{c(MPO)}$ coefficients and the native MPO phases. Four water molecles in the native MPO distal heme cavity were removed from the model prior to calculating the native MPO structure factors. A model of SHA based on an X-ray crystal structure reported by Larsen (1978) was

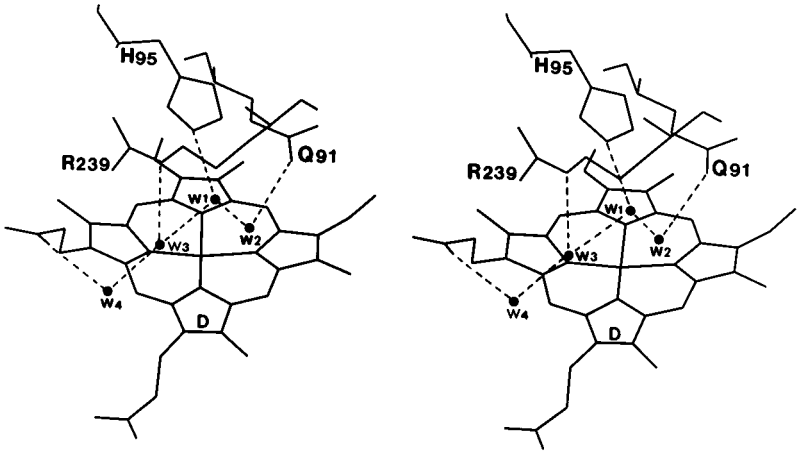


FIGURE 2: Observed hydrogen-bonding pattern for four water molecules in the distal heme cavity of one half of native human MPO. W1 is 2.7 Å from the His 95 $N_E$ and 3.1 Å from the heme iron. In the alternative configuration, the two hydrogen bonds shown between Gln 91 and W2 and W1 and W3 are replaced by hydrogen bonds between Gln 91 and W1 and W2 and W3.

manually fitted to the observed density in this difference map. A water molecule was also added to the model in density that was observed close to the position previously occupied by one of the four water molecules omitted from the native MPO model.

The model for the MPO−SHA complex was then refined at 2.3 Å resolution by energy minimization and simulated annealing using the X-PLOR program (Brunger, 1988). Stereochemical restraints for the SHA molecule involved bond lengths and angles reported by Larsen (1978) with free rotation about the C6−C7 and C7−N8 bonds. Following refinement, $2F_o - F_c$ and $F_o - F_c$ maps were calculated and examined for additional features that had not been included in the model. As an additional check that the positions of amino acid side chains close to the SHA binding site had not undergone large conformational changes, an omit map was calculated. One hundred fifty cycles of conjugate gradient refinement were performed on a model from which we omitted the side chains of amino acids in the immediate environment of the bound inhibitor: Gln 91, His 95, Phe 99, Arg 239, Phe 366, and Phe 407 in both halves of the molecule. The least squares superposition algorithm in the X-PLOR program package was then used to superimpose the coordinates of the native enzyme and the inhibitor complex in order to detect any significant conformational changes. A more detailed search for conformational differences was carried out by superimposing the active site regions comprising: the heme, water 4, and residues Q91, D94, H95, F99, R239, E242, M243, H336, F366, and F407. Since the two apparently identical halves (A and B) of the MPO molecule are crystallographically independent, differences between the two halves can be used to estimate the level of errors in the final coordinates.

## RESULTS

Crystals of the MPO−SHA complex have unit cell dimensions ($a = 111.6$ Å, $b = 64.6$ Å, $c = 93.5$ Å, and $\beta = 97.3°$) which are very similar to those of the native enzyme ($a = 111.7$ Å, $b = 64.6$ Å, $c = 94.2$ Å, and $\beta = 97.9°$). This allowed the structure of the complex to be determined using difference Fourier methods. The initial $F_{o(MPO-SHA)} - F_{c(MPO)}$ difference map showed positive density with maxima of $10.9\sigma$ and $9.9\sigma$ corresponding to the bound SHA in the distal heme cavities of each half of the molecule. As shown in Figure 3, the difference electron density profile allowed unambiguous modeling of the SHA molecule. An additional positive peak ($6.4\sigma$ and $6.2\sigma$ in each half) appeared close to the position of one of the four water molecules which had been removed from the native model, and this water was added to the MPO−SHA model. The difference map showed no further positive or negative features greater than $3\sigma$ in the vicinity of the distal heme pocket. Since there are small differences between the unit cell dimensions of the complex and the native enzyme, the structures were superimposed to compare their conformations. Coordinate differences on the order of 0.5 Å were confined to the solvent-exposed surface of the molecule, particularly in the B half.

The SHA molecule displaces three water molecules from the distal heme pocket of the native enzyme, and a fourth water molecule is shifted about 0.37 Å from its location in the native structure. There do not appear to be any significant active site protein conformational changes associated with SHA binding. Superposition of the active site regions of the native and the inhibitor complex gave an rms difference in atomic coordinates of 0.13 Å in each half of the molecule. This is a lower value than is found for superposition of the A and B active site regions of the native (0.16 Å) or the inhibitor complex (0.17 Å). The greatest shift was seen for water 4 which moved 0.38 and 0.36 Å in the same direction in each half of the molecule. All other atomic shifts were less than 0.3 Å and did not show a consistent pattern for the two halves. We therefore conclude that there are no significant conformational changes in the active site region when SHA binds, other than displacement of three water molecules and a small shift in the position of a fourth water molecule.

As predicted by earlier model building studies (Hori et al., 1994), the aromatic ring binds to a hydrophobic region at the entrance to the distal cavity. The plane of the aromatic ring is tilted about 20° with respect to that of the heme pyrrole ring D which forms the lower surface of the hydrophobic cavity, while the $\beta$, $\gamma$, and $\delta$ carbons of Arg 239 form the upper surface. Additional van der Waals interactions occur with adjacent phenylalanines Phe 99, Phe 366, and Phe 407, each of which has an aromatic ring carbon atom within 4.2−4.6 Å of the aromatic ring of the SHA molecule. The hydroxamic acid group lies in the center of the distal cavity between the distal histidine and the heme iron, and both the carbonyl and hydroxyl oxygens form hydrogen bonds with amino acid side chains in the distal

Table 1: Distal Cavity Hydrogen Bond Distances[a]

| | native MPO | | | MPO−SHA complex | | |
|---|---|---|---|---|---|---|
| from | to | A | B | to | A | B |
| H95$N_E$ | W1 | 2.76 | 2.67 | SHA-O8 | 2.70 | 2.52 |
| Q91$N_E$ | W1 | 3.10 | 3.48* | SHA-O8 | 3.07 | 3.38 |
| Q91$N_E$ | W2 | 3.96* | 3.03 | SHA-O7 | 2.90 | 2.75 |
| R239$N_E$ | W3 | 3.36 | 3.31 | SHA-O1 | 3.64 | 3.40 |
| W4 | W3 | 2.76 | 2.95 | SHA-O1 | 2.61 | 2.75 |
| HEM(O)[b] | W4 | 2.76 | 2.59 | W4 | 2.67 | 2.61 |
| W1 | W2 | 2.75 | 2.70 | | | |
| W2 | W3 | 3.32 | 3.59* | | | |
| W1 | W3 | 3.60* | 3.20 | | | |
| W3 | W4 | 2.76 | 2.95 | | | |

[a] Distances in angstroms between pairs of atoms involved in the hydrogen-bonding network in the distal heme cavities of native MPO and the MPO−SHA complex. A and B refer to the two halves of the MPO model. Distances for non-hydrogen bonding pairs in the two alternative configurations are indicated by *. [b] HEM(O) = heme pyrrole ring C proprionate carboxyl oxygen.

cavity. These hydrogen bonds replace those that involved two of the water molecules displaced from the native enzyme.

In the native enzyme, a group of four water molecules (W1−W4) occupies the distal heme cavity. In the refined model for the native enzyme, the positions of two of these water molecules (W1 and W2) differ in the two chemically identical but crystallographically unrelated halves of the molecule. When the active site regions (comprised of the heme, ten amino acids, and four water molecules) of the two halves of the molecule are superimposed, the positions of W1 and W2 in the A and B halves differ by 0.55 and 0.85 Å, respectively. By comparison, pairs of atoms from the protein and the heme show differences of less than 0.5 Å and the rms difference for all atoms used in the superposition is 0.16 Å. These differences in the positions of water molecules W1 and W2, presumably resulting from the differential effects of crystal packing forces on the two halves of the molecule, give rise to two different hydrogen-bonding patterns (Table 1). Above average values for the temperature factors of these four water molecules suggest that they participate in a relatively loose pattern of hydrogen bonds. One possible hydrogen-bonding pattern for the group of four water molecules (W1−W4) in the distal cavity of the native enzyme is shown in Figure 2. In the center of the pocket, water molecule W1 is hydrogen bonded to the $N_E$ nitrogen of the distal histidine 95. While this water molecule lies between the distal histidine and the heme iron, it is not liganded to the iron, since the Fe−O distance of 3.1 Å is much greater than the ligand−iron distances typically observed for peroxidases (Edwards & Poulos, 1990). Water molecule W1 is also hydrogen bonded to two more water molecules, W2 and W3, at the entrance to the distal cavity. The second water molecule, W2, is hydrogen bonded to the amide group of Gln 91, while the third water, W3, appears to interact weakly with the guanidinium group of Arg 239, since the distances to the $N_E$ and $NH_2$ nitrogens of the guanidinium group (3.3−3.4 Å) are at the upper limit of the range normally seen for hydrogen bonding. A fourth water molecule, W4, is hydrogen bonded to W3 and also to one of the carboxyl oxygens of the proprionate group attached to the heme pyrrole ring C.

In the MPO−SHA complex, water moleculs W1−W3 are displaced by the SHA molecule. Oxygen atoms O7, O8, and O1 of SHA are positioned close to the sites occupied by W1−W3 in the native enzyme (Figure 4). The carbonyl O7 is a hydrogen bond acceptor for an amide proton of Gln 91, while the O8 hydroxyl acts as a hydrogen bond donor to the $N_E$ nitrogen of the distal histidine. In the native enzyme crystal structure, the orientation of the amide group of Gln 91 is ambiguous since its hydrogen bond donor−acceptor characteristics cannot be determined. This amide forms a hydrogen bond with water molecule W2 and also makes the sole hydrogen-bonding interaction with the amide group of Gln 88. The carbonyl oxygen of SHA that replaces W2 in the inhibitor complex can only act as a hydrogen bond acceptor and therefore must be hydrogen bonded to the Gln 91 amide $NH_2$, thereby establishing unique orientations for both the Gln 91 and Gln 88 amide groups. The O1 salicyl ring hydroxyl oxygen is hydrogen bonded to the fourth water molecule which is shifted 0.37 Å from its position in the native enzyme but remains hydrogen bonded to the pyrrole ring C proprionate carboxyl group. There is no indication of any significant movement of the guanidinium group of Arg 239, and hydrogen bonding with the hydroxamic acid ring hydroxyl must be very weak since the $N_E$−OH distances are 3.64 and 3.40 Å in the two halves of the molecule. The hydroxamic acid nitrogen is 3.5 Å from the heme iron, and this NH group appears to form an intramolecular hydrogen bond with the carbonyl oxygen, as is found in the X-ray crystal structure of SHA (Larsen, 1978).

## DISCUSSION

Salicylhydroxamic acid can be characterized as a bisubstrate analogue inhibitor of MPO since the hydroxamic acid group is structurally analagous to the peracid substrates for compound **I** formation and the salicyl group is structurally similar to the aromatic alcohols and amines that are substrates for the single-electron reductions of compounds **I** and **II**. Typically, inhibitors of this type have high binding affinities because binding involves two separate interactions with the enzyme. The high binding affinity of BHA to HRP has been attributed to a combination of polyfunctional hydrogen bonding between the hydroxamic acid group and amino acid residues in the distal cavity and hydrophobic interactions involving the aromatic ring (Schonbaum, 1973). These two aspects of binding are clearly exemplified in the SHA−MPO complex. Hydrogen bonds between the hydroxamic acid group and the distal His 95 and Gln 91 of MPO replace those formed by two water molecules in the native enzyme, while a separate hydrophobic interaction occurs between the aromatic ring and a hydrophobic region at the entrance to the distal heme cavity.

The low-temperature (77 K) EPR spectrum of native human MPO is altered upon BHA or SHA binding (Ikeda-Saito et al., 1991; Hori et al., 1994). The native enzyme exhibits a predominantly high-spin EPR signal ($g$ = 6.74, 5.18, and 1.97), while the complexes show both high-spin ($g$ = 6.99, 4.93, and 1.95) and low-spin ($g$ = 2.66, 2.22, and 1.81) components. The low-spin component is not observed in complexes of MPO with 4-amino salicylate, phenol, *p*-cresol, or resorcinol. In contrast, room-temperature optical spectra of BHA and SHA complexes of MPO show that the heme iron is in a predominantly high-spin state (Ikeda-Saito et al., 1991). These results were interpreted in terms of a weak liganding interaction between the hydroxamic acid nitrogen and the heme iron and a temperature-dependent spin state transition in the hydroxamic acid complexes (Hori et al., 1994). In the X-ray crystal structure of the MPO−SHA complex, there is no evidence for a sixth

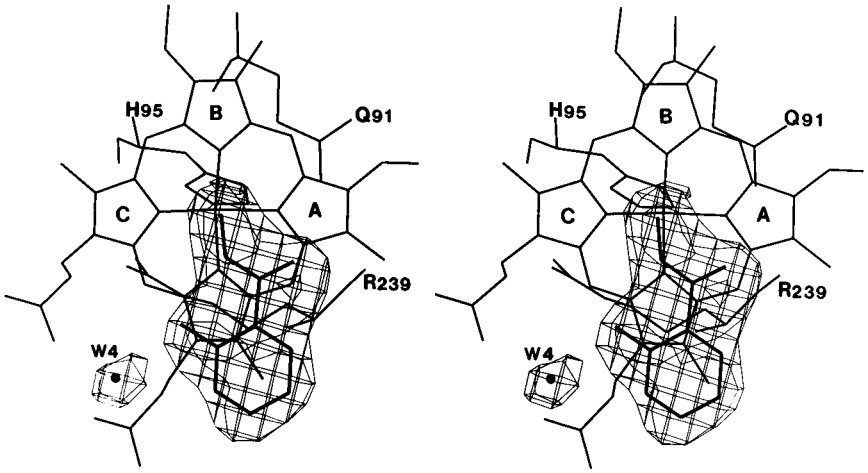


FIGURE 3: Refined model for SHA superimposed on the $F_o - F_c$ map used to fit the model. The contour level is 1.7$\sigma$. SHA binds between the heme pyrrole ring D and the side chain of Arg 239. Positive density is also seen for the water molecule (W4) that was omitted from the phasing model.

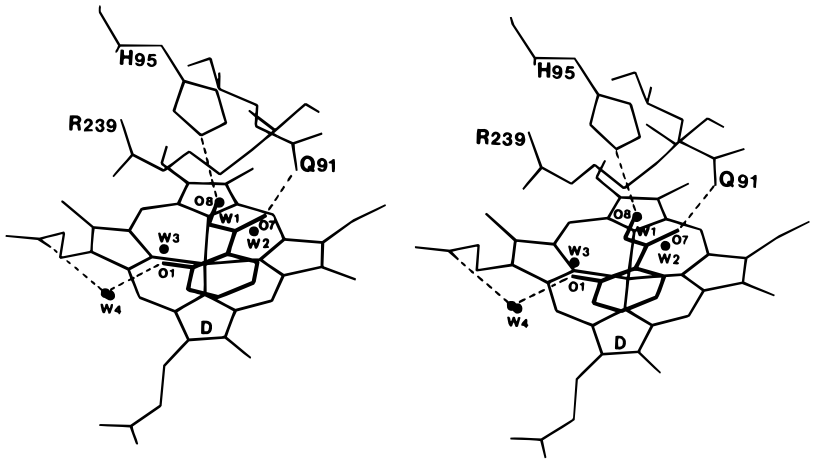


FIGURE 4: Model for SHA bound to human MPO. The positions of the three oxygen atoms of SHA are close to the positions occupied by three water molecules (W1, W2, and W3) displaced from the native enzyme. Water (W4) is shifted about 0.35 Å from its position in the native structure.

ligand to the iron. The hydroxamic acid hydroxyl oxygen and NH nitrogen are 3.1 and 3.5 Å away from the iron, respectively, and the NH group probably participates in an intramolecular hydrogen bond with the salicyl ring hydroxyl oxygen, as is seen in the crystal structure of SHA. Thus, while there are no direct liganding interactions to the iron, the local electrostatic environment is likely to be altered by SHA binding and this may explain the small changes seen in the high-spin EPR signals from the heme iron.

It has previously been suggested that the 3 orders of magnitude difference between the dissociation constants for BHA and SHA binding to MPO could result from additional hydrogen bonding between the aromatic ring hydroxyl of SHA and an amino acid side chain on the protein (Ikeda-Saito et al., 1991). In the MPO-SHA crystal structure, the salicyl ring hydroxyl group of SHA participates in hydrogen bonding to the guanidinium group of Arg 239 and also to the water molecule (W4) which is in turn hydrogen bonded to the pyrrole ring C proprionate carboxyl group. If BHA binding also results in the displacement of three water molecules from the distal cavity, then the loss of hydrogen bonds associated with W3 in the native enzyme could explain the weaker binding of BHA compared with that of SHA.

While the physiological role of MPO is associated with catalysis of a two-electron oxidation of chloride ion to hypochlorite, it can also catalyze the single-electron oxidation of a variety of aromatic alcohols and amines. For HRP, it has been proposed that single-electron, single-proton oxidations of aromatic alcohols and amines take place at the heme periphery. Measurements of the transfer nuclear Overhauser effect for HRP complexes with BHA, resorcinol, and 2-methoxy-4-methylphenol indicated that the nonexchangeable aromatic ring protons are within 4 Å of the heme pyrrole ring D 8-methyl protons and 8−11 Å from the heme iron (Sakurada et al., 1986). In addition, free radical products of the reaction of phenylhydrazine with HRP yield $\delta$-mesophenyl and 8-hydroxymethyl derivatives, again suggesting that oxidation occurs at the heme edge, in the vicinity of the $\delta$-meso carbon and the 8-methyl group on pyrrole ring D (Ator et al., 1987; Ator & Ortiz de Montellano, 1987). Proton relaxation NMR studies of aromatic substrate molecules, including phenol, *p*-cresol, resorcinol, aniline, and *p*-toluidine, bound to lactoperoxidase (LPO) indicated distances of 9.4−11.1 Å from the ring protons to the iron (Modi et al., 1989). These authors also concluded that the aromatic rings were inclined rather than parallel with respect to the heme plane because the distances of different protons in the ring to the iron were not greatly different. In the MPO−SHA complex, the aromatic ring is almost centered above the pyrrole ring D 8-methyl group such that each carbon atom in the aromatic ring is about 4.1 Å from the 8-methyl carbon, in good agreement with the proton−proton distances

of less than 4 Å reported for the HRP complexes. However, the distances from the salicyl ring carbon atoms to the heme iron in the MPO−SHA complex range from 6.4 to 7.7 Å, considerably shorter than the ring proton to heme iron distances determined for either the HRP or LPO complexes. The most significant difference between our result and the conclusions reached by NMR studies of HRP and LPO complexes is that in MPO the orientation of the aromatic ring with respect to the heme plane is almost parallel rather than perpendicular. While the aromatic ring binding site in the nonhomologous HRP may well differ from that in MPO, amino acid residues in the heme environment are highly conserved between the homologous mammalian peroxidases MPO and LPO, suggesting that the mode of aromatic substrate binding should be very similar in these two enzymes.

The binding of SHA to MPO is also expected to closely resemble the binding of aromatic peracids that, like hydrogen peroxide, promote compound **I** formation in heme peroxidases. The MPO−SHA complex can therefore be considered as a model for the prereaction complex formed between an aromatic peracid and MPO. Aromatic peracid binding would displace three water molecules from the distal heme cavity upon formation of a hydrogen bond between the peracid proton and the distal histidine. The formation of this hydrogen bond is thought to represent the first step in the deprotonation of the peracid to yield an anionic intermediate that can interact directly with the heme iron. The dependence of this process on the protonation state of the distal histidine accounts for the lower limit on the pH dependence of compound **I** formation in peroxidases. The SHA NH group analogue of the peracid $O_{(1)}$ does not participate in hydrogen bonding with the enzyme in our model of the inhibitor complex. This nitrogen is close to the heme pyrrole ring D nitrogen (3.0 Å) and to the distal histidine $N_E$ (3.2 Å) but is at least 4 Å away from the guanidinium group of Arg 239. The hydroxamic acid group of SHA in the MPO−SHA complex is rotated by about 8° with respect to the plane of the aromatic ring. This near coplanar orientation may be partly due to restraints incurred by the internal hydrogen bond between the NH and the ring hydroxyl group. For BHA and aromatic peracids lacking the ring hydroxyl group, some rotation could occur about the C6−C7 bond as is observed in the crystal structure of iron(III) (benzohydroxamate)$_3$ trihydrate where the three hydroxamate groups are rotated 9.4, 20.7, and 39.1° with respect to the planes of their benzene rings (Lindner & Gottlicher, 1969). According to our model, movement of the arginine side chain in addition to some rotation about the C6−C7 bond would be required for hydrogen bond formation between the guanidinium group and the $O_{(1)}$ of a bound aromatic peracid. However, movement of the Arg 239 side chain is constrained by a salt bridge interaction with Asp 237 and additionally by van der Waals contacts with the aromatic ring of Phe 99. In CCP, movement of the corresponding distal Arg 48 side chain toward a heme ligand has only been observed in complexes containing a monatomic anion bound to the heme iron (Edwards et al., 1984, 1987). These observations, together with the finding that an Arg 48 Lys mutant of CCP exhibited only a 2-fold reduction in the rate of compound **I** formation, led to the proposal that the primary role for the distal arginine in heme peroxidases is to stabilize the oxyferryl center (Vitello et al., 1993; Miller et al., 1994).

All of the heme−ligand complexes of CCP for which X-ray crystal structures have been determined involve direct ligation at the sixth coordination site of the heme iron, with iron−ligand distances of 1.8−2.2 Å. Formation of compound **I** requires deprotonation of the peroxide $O_{(2)}$ hydroxyl to yield a transient $Fe^{III}$−OOH intermediate prior to scission of the O−O bond. The crystal structure of an $Fe^{II}-O_2$ dioxygen complex of the Trp 191 Phe mutant of CCP has been described as an analogue of this short-lived intermediate which has an estimated half-life of no greater than 0.7 ms in cytochrome *c* peroxidase (Miller et al., 1994). In contrast, the MPO−SHA complex provides a basis for modeling a prereaction complex in which hydrogen peroxide donates a hydrogen bond to the distal histidine prior to deprotonation and heterolysis of the O−O bond. The initial interaction of hydrogen peroxide with MPO is likely to involve displacement of water molecule W1 as the $O_{(2)}$ hydroxyl donates a hydrogen bond to the unprotonated distal histidine. The rapid rate of hydrogen peroxide binding may be explained by additional hydrogen bonding between the $O_{(1)}$ hydroxyl and water molecules W2 and W3, which may shift positions slightly, but are unlikely to be displaced from the distal pocket.

The organization of catalytically significant amino acid residues and water molecules in the distal heme pockets of CCP and MPO are very similar. The distal His 95 and Arg 239 in MPO have counterparts in His 52 and Arg 48 of CCP. While Gln 91 of MPO is replaced by Trp 51 in CCP, both can act as hydrogen bond donors. Water molecules W1−W3 have counterparts WAT 595, WAT 596, and WAT 648 in CCP, and the hydrogen-bonding pattern between these water molecules and the three active site amino acids is essentially identical. In both peroxidases, one water molecule is a hydrogen bond donor to the distal histidine, a second accepts a hydrogen bond from the distal Arg, while the third accepts a hydrogen bond from the Gln 91 amide in MPO and from the Trp 51 NH in CCP. Thus, the most significant features of the proposed transient intermediate in CCP have analagous counterparts in MPO. Deprotonation of $H_2O_2$ is a prerequisite for the formation of this intermediate that is characterized by a short O−Fe ligand distance of 1.8 Å in the analogous $Fe^{II}$−CCP dioxygen complex (Miller et al., 1994). In contrast, the SHA−MPO complex provides a basis for modeling the prereaction complex of $H_2O_2$ with the enzyme prior to deprotonation. The sequence of events in compound **I** formation can be represented by the following steps:

$$E^{*}H_2O(Fe^{III}) + H_2O_2 \rightarrow E^{*}H_2O_2(Fe^{III}) + H_2O \quad (1)$$

$$E^{*}H_2O_2(Fe^{III}) \rightarrow E{-}H^{+}(Fe^{III}{-}OOH) \quad (2)$$

$$E{-}H^{+}(Fe^{III}{-}OOH) \rightarrow E^{+}(Fe^{IV}{=}O) + H_2O \quad (3)$$

where * represents a hydrogen bond with the distal histidine and $E^+$ an enzyme-bound porphyrin $\pi$-cation radical for MPO and a Trp 191 radical for CCP. Step 2 above involves conversion of the prereaction complex to the transient intermediate, necessitating a significant movement of the deprotonated $O_{(2)}$ on the order of 1.2 Å upon liganding to the sixth coordination site of the heme iron.

Miller et al. (1994) postulated the significance of two oxygen binding locations termed $O_A$ and $O_B$ in the ferrous CCP dioxygen complex. Simultaneous occupation of both

sites is postulated to be possible only for covalently linked oxygen atoms and not by two water molecules. Thus, in the resting enzyme, a water molecule occupies site $O_B$, while site $O_A$, the sixth coordination position of the heme iron, is vacant. Conversely, occupation of site $O_A$ by the ferryl iron oxygen ligand, following cleavage of the O−O bond, forces a water molecule formed by reprotonation of $O_{(1)}$ at the $O_B$ site to be expelled from the distal cavity. One consequence of the two-site model is that Fe−$O_{(2)}$ bond formation and deprotonation of $O_{(2)}$ by the distal histidine cannot be considered as simultaneous events, since they require $O_{(2)}$ to occupy quite different sites that are about 1.2 Å apart. We therefore propose that the protonated $O_{(2)}$ occupies site $O_B$ in the prereaction complex and must migrate to the second site ($O_A$) to bind to the iron following deprotonation by the distal histidine. In the model for the transient $Fe^{III}$−OOH intermediate of CCP, the oxygen at site $O_B$ has tetrahedral geometry, forming hydrogen bonds with both WAT 596 and WAT 648. Similarly, in our model for the prereaction complex, $O_{(1)}$ can hydrogen bond to the analagous water molecules W2 and W3. Thus, site $O_B$ can be regarded as a binding location for proton donors to the distal histidine, while site $O_A$ favors binding of deprotonated ligands such as $^-$OOH, $CN^-$, and NO at the sixth coordination site of the heme iron. A third oxygen binding site is required for the initial binding of $O_{(1)}$ in the prereaction complex. This site has not yet been observed directly in a crystal structure complex but is presumably located close to the position of the nitrogen atom of SHA in the MPO−SHA complex and likely involves hydrogen bonding to water molecules W2 and W3 that are in turn hydrogen bonded to Gln 91 (Trp 51 in CCP) and the distal Arg in the resting enzyme. This postulated third site is presumably also only accessible to an oxygen atom covalently bound to a second oxygen that occupies site $O_B$. Expulsion of the water molecule formed by protonation of $O_{(1)}$ following scission of the O−O bond implies that neither site $O_B$ nor the postulated third site can be occupied by a water molecule when site $O_A$ is occupied by the ferryl oxygen of compound **I**.

In conclusion, the mechanisms of Compound **I** formation in the mammalian peroxidases represented by MPO and the fungal peroxidases represented by CCP are likely to be very similar. The MPO−SHA complex appears to represent a model for a prereaction complex for the initial interaction of hydrogen peroxide with peroxidases. Following deprotonation, the $O_{(2)}$ oxygen of this substrate must move about 1.2 Å to ligand directly to the heme iron in forming a transient intermediate that is modeled by the dioxygen complex of ferrous CCP.

## ACKNOWLEDGMENT

We thank Dr. Nils Peder Willassen for the generous gift of the human MPO used in this work, Dr. Michael Chapman for use of the R-axis II image plate system for X-ray data collection, and Dr. Ann English for helpful discussions and comments on the original manuscript.

## REFERENCES

Agner, K. (1941) *Acta Chem. Scand. 2* (Suppl. 8), 1−62.

Andrews, P. C., & Krinsky, N. I. (1981) *J. Biol. Chem. 256*, 411−418.

Ator, M. A., & Ortiz de Montellano, P. R. (1987) *J. Biol. Chem. 262*, 1542−1551.

Ator, M. A., David, S. K., & Ortiz de Montellano, P. R. (1987) *J. Biol. Chem. 263*, 14954−14960.

Belding, M. E., Klebanoff, S. J., & Ray, C. G. (1970) *Science 167*, 195−196.

Brunger, A. J. (1988) *J. Mol. Biol. 203*, 803−816.

Cals, M.-M., Mailliart, P., Brignon, G., Anglade, G., & Dumas, B. R. (1991) *Eur. J. Biochem. 198*, 733−739.

Davies, B., & Edwards, S. W. (1989) *Biochem. J. 258*, 801−806.

Dolphin, D., Forman, A., Borg, D. C., Fajer, J., & Felton, R. (1971) *Proc. Natl. Acad. Sci. U.S.A. 68*, 614−618.

Edwards, S. L., & Poulos, T. L. (1990) *J. Biol. Chem. 265*, 2588−2595.

Edwards, S. L., Poulos, T. L., & Kraut, J. (1984) *J. Biol. Chem. 259*, 12984−12988.

Edwards, S. L., Xuong, N.-h., Hamlin, R. C., & Kraut, J. (1987) *Biochemistry 26*, 1503−1511.

Fenna, R., Zeng, J., & Davey, C. (1995) *Arch. Biochem. Biophys. 316*, 653−656.

Finzel, B. C., Poulos, T. L., & Kraut, J. (1984) *J. Biol. Chem. 259*, 13027−13036.

Harrison, J. E., & Schultz, J. (1976) *J. Biol. Chem. 251*, 1371−1374.

Hori, H., Fenna, R. E., Kimura, S., & Ikeda-Saito, M. (1994) *J. Biol. Chem. 269*, 8388−8392

Ikeda-Saito, M., Shelly, D. A., Lu, L., Booth, K. S., Caughey, W. S., & Kimura, S. (1991) *J. Biol. Chem. 266*, 3611−3616.

Kimura, S., & Yamazaki, I. (1979) *Arch. Biochem. Biophys. 198*, 580−588.

Kimura, S., & Ikeda-Saito, M. (1988) *Proteins: Struct., Funct. Genet. 3*, 113−120.

Kitagawa, T., Hashimoto, S., Teraoka, J., Nakamura, S., Yajima, H., & Hosoya, T. (1983) *Biochemistry 22*, 2788−2792.

Klebanoff, S. J. (1970) *Science 169*, 1095−1097.

Kunishima, N., Fukuyama, K., Matsubara, H., Hatanaka, H., Shibano, Y., & Amachi, T. (1994) *J. Mol. Biol. 235*, 331−344.

La Mar, G. N., Hernandez, G., & de Ropp, J. S. (1992) *Biochemistry 31*, 9158−9168.

Larsen, I. K. (1978) *Acta Crystallogr. B34*, 962−964

Lindner, H. J., Gottlicher, S. (1969) *Acta Crystallogr. B25*, 832−842.

Loo, S., & Erman, J. E. (1975) *Biochemistry 14*, 3467−3470.

Miller, M. A., Shaw, A., & Kraut, J. (1994) *Struct. Biol. 1*, 524−531.

Modi, S., Digambar, V., Mitra, B., & Mitra, S. (1989) *Biochim. Biophys. Acta 996*, 214−225.

Poulos, T. L., & Kraut, J. (1980a) *J. Biol. Chem. 255*, 8199−8205.

Poulos, T. L., & Kraut, J. (1980b) *J. Biol. Chem. 255*, 10322−10330.

Poulos, T. L., Freer, S. T., Alden, R. A., Edwards, S. L., Skogland, U., Takio, K., Eriksson, B., Xuong, N., Yonetani, T., & Kraut, J. (1980) *J. Biol. Chem. 255*, 575−580.

Poulos, T. L., Edwards, S. L., Wariishi, H., & Gold, M. H. (1993) *J. Biol. Chem. 268*, 4429−4440.

Sakurada, J., Takahashi, S., & Hosoya, T. (1986) *J. Biol. Chem. 261*, 9657−9662.

Schonbaum, G. R. (1973) *J. Biol. Chem. 248*, 502−511.

Schonbaum, G. R., & Lo, S. (1972) *J. Biol. Chem. 247*, 3353−3360.

Smulevich, G., Wang, Y., Mauro, J. M., Fishel, L. A., Kraut, J., & Spiro, T. G. (1991) *Biochemistry 30*, 9546−9558.

Stump, R., & Oliver, J. (1985) *Biophys. J. 47*, 82a.

Sutton, B. J., Little, C., Olsen, R. L., & Willassen, N. P. (1988) *J. Mol. Biol. 199*, 395−396

Thanabal, V., de Ropp, J. S., & La Mar, G. N. (1987) *J. Am. Chem. Soc. 109*, 7516−7525.

Vitello, L. B., Erman, J. E., Miller, M. A., Wang, J., & Kraut, J. (1993) *Biochemistry 32*, 9807−9818.

Welinder, K. G. (1985) *Eur. J. Biochem. 151*, 497−504.

Yonetani, T., & Schleyer, H. (1967) *J. Biol. Chem. 242*, 1974−1979.

Zeng, J., & Fenna, R. E. (1992) *J. Mol. Biol. 226*, 185−207.

BI960577M